13th ewtec 2019 Proceedings of the 13th European Wave and Tidal Energy Conference 1-6 Sept 2019, Naples, Italy

Assessment of tidal turbine load cycles using synthesised load spectra, including blade-scale fluctuations

Hannah R. Mullings and Tim Stallard

***Abstract*—Tidal turbines are currently being utilised for electrical generation in test facilities and small scale array sites. The aim of this study is to evaluate the impact of synthesised turbulence loads and waves, on load spectra and on damage equivalent loads for a typical tidal resource. The impact is assessed through the understanding of several unsteady flow phenomena, such as distortion of the turbulence and blade-generated unsteadiness for a selected quasi-steady flow case as well as operational conditions. The overall loading is determined here through the use of damage equivalent loads (DEL), these loads utilise Rainflow cycle counting over the load time history to give the number of load cycles. By including the magnitude of the load fluctuations due to blade-scale flow onto the load spectra, results in an increase of the number of cycles to within 1% of experimental comparison case with a 17% variation in DEL.**

***Index Terms*—Blade Loading, Spectral Turbulence, Tidal Turbine.**

I. Introduction

UNLIKE wind turbines, tidal turbines are typically located in a more complex working fluid. Due to the influence of waves, directionally varying velocity and varying spatial and temporal turbulence scales, they therefore experience higher cyclic loading. Increased cyclic loading causes fatigue of components before material failure due to ultimate loading.

An approach to determining lifetime loading due to turbulent tidal stream conditions would be to conduct field trials over a long period of time, e.g. ten years, and analyse the recorded data. However such tests are extremely costly and are of limited value to informing system design. Component design life may be assessed based on load cycles experienced during a number of quasi-steady intervals [1], [2]. It is widely recognised that improved understanding is required of the characteristics of turbulence at tidal stream sites and the influence of such flows on turbine design. The characteristics of tidal stream turbulence has been studied through analysis of data from test sites [3], laboratory scale studies of turbine loading [4], [5] and modelling at various levels of complexity ranging from blade element studies through to industrial scale CFD [6], [7].

This is paper number 1691, conference track - Tidal Hydrodynamic Modelling

This work was supported by the EPSRC, as well as an additional scholarship from the University of Manchester.

H. R. Mullings is at The University of Manchester, Oxford Road, Manchester, M13 9PL (e-mail: hannah.mullings@manchester.ac.uk).

T. Stallard is at The University of Manchester, Oxford Road, manchester, M13 9PL (e-mail: tim.stallard@manchester.ac.uk).

Using the predictability of the tidal resource, an understanding of mean onset flow conditions in coastal locations can be determined through the use of tidal constituents, this is shown in Fig. 1 for the Meygen Site in Pentland Firth. This range of onset flow would correspond to a variation in turbulence characteristics and hence magnitude of loading. One way of analysing longer term loading is to consider a series of quasi-steady states. Ten minute sampling has been used [8] to divide a range of sea-states. For each quasi-steady state a thorough understanding of the environmental and operational conditions is needed to inform the frequency dependence of loads. Understanding these conditions and the influence on load cycles will help to inform the design of turbine components in other site locations, if only some of the environmental conditions are known. In this work a spectral turbulence model has been used to describe the underlying onset flow at one quasi-steady flow case. Additional environmental and operational factors that are known to contribute to unsteady loading have then been applied and assessed with comparison to an experimental load spectra. The experimental data is obtained from tests conducted as part of the XMED project, with a description of the turbine and the frequency dependence of mean loads on the turbine found in [9]. The influence of array positioning onto the overall loading has been considered in [10], with the focus here on determining the longer term loading using multiple quasi-steady cases for single turbine.

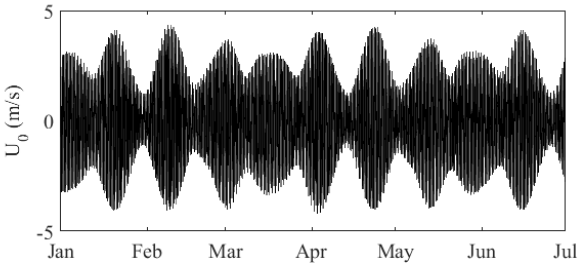

Fig. 1. Example of a nine constituent model used to generate six months of onset flow data, U_0 in the Pentland Firth.

Previous work has been conducted examining the influence of some of the operational conditions onto the loading of tidal turbine components. The influence of the turbulent flow field has been initially examined by [11] following their understanding from wind loading highlighted how fatigue loading can be examined for blade loading under variable sea states. Elasha et

al. 2015 [12] examined the influence of turbulence and shear on the design life of a gearbox and [13] compared the influence of turbulence on the performance of blades. Wave loading has also been examined from a series of regular wave conditions in [11] with a progression through to fatigue calculations, and [14] examined the in-plane and out-of-plane bending moments due to waves and yaw, but without the inclusion of the long term loading effects on overall design life of blades. Some work has been conducted in trying to utilise large ranges of environmental conditions to inform fatigue calculations, [15]. However the basis of that work used a scaled experimental spectrum of loads, this data is not always available. Hence an efficient process is shown here which utilises the a spectral turbulence model with a range of environmental conditions to determine loading through a blade element model.

II. Method

A. Quantifying Loads

Cyclic loading can be assessed using a load spectrum to identify the operational and environmental factors that cause peak loading and at specific frequencies.

Damage Equivalent Loads (DEL) are a function of the magnitude and number of the load cycles found combined with a longer term time period, which provides a specific load which oscillates at a singular frequency. The calculation also depends on the material of the components; here for comparison between methods and experiment the single frequency will be kept constant. For the blade loading case, the rotor frequency f_0 is chosen, for the rotor loading the blade passing frequency of $3f_0$ is chosen.

$$DEL = \left(\frac{\sum_i n_i {L_i}^m}{fT} \right)^{\frac{1}{m}} \tag{1}$$

Where L_i is the load at bin 'i', m is a material property given by the slope of the S-N curve for the material, T is the length of time for operation, f is the repetition frequency, n_i is the number of cycles at given load, obtained through the Rainflow cycle counting. In this case the method by [16] is used, in which if the specific material is not known a material gradient is chosen which is representative. Here $m = 10$ is used for blade loading, which is the material gradient for a semi-flexible material such as fibre glass and $m = 4$ is used for the rotor loading representing a stiff material such as steel.

B. Operational Conditions

The conditions in which a tidal turbine operates have initially been assessed through an examination of conditions which effect wind loading. Work conducted by Leishman, [17], listed the factors effecting wind turbines by dividing into periodic and aperiodic components. Based upon this work the periodic/deterministic factors are: Onset flow speed, shear, tower shadow, yaw and random/aperiodic factors which effect the loading are turbulence, wake dynamics, blade/wake interactions and waves. In this study the deterministic loads are calculated for comparison with the experimental case, with one turbulence case. A blade root bending moment spectra obtained from the experimental results and normalised by the rotor frequency is shown in Fig. 2.

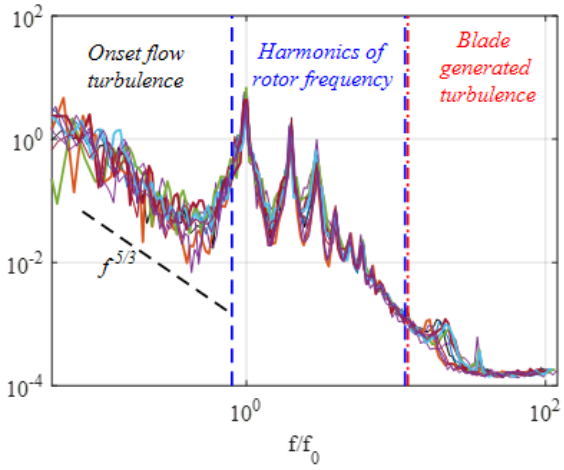

Fig. 2. Normalised root bending moment spectra from experimental data, XMED project, with frequency ranges highlighted showing the different influencing factors on the loads.

This highlights the range of influence for the turbulence, the high frequency fluctuations and the mid-frequency range dominated by the rotor harmonics. The work in this section is to establish the operational conditions which contribute to the loads at the rotor harmonics, the cause of the high frequency fluctuations will be examined in Section III-A.

C. Turbulence Modelling

The onset variation of flow to the turbine can be considered as a mean value and the thrust and power coefficients can be determined through blade element momentum theory, (BEM). However if the load spectra is be examined to determine the influence of different operational factors at various frequencies the background ambient turbulence should be included. There are many different methods used to model background turbulence, such as von Kármán and Kaimal, [18]. These have been developed primarily for use in aerospace applications as a model of wind turbulence. In this case the von Kármán model has been chosen for the generation of turbulence in the three linear velocity components (u,v,w). This has been determined for domain which size correlates to the experimental set up which corresponds to the comparison data. The characteristics of the turbulent flow field have also been determined from the experimental case and used as input to the generation of the von Kármán flow field, this has been created using the commercial software Tidal Bladed, [19].

The data extracted from Tidal Bladed produces a grid of turbulent velocity components, this grid is then considered as a time varying onset flow field to the turbine. The turbulent characteristics which where used to define the onset flow are recalculated after generation,

with the turbulence intensity kept at exactly 3% and the variation in length scale given in Table II-C.

The length scale in the von Kármán case has been determined through the use of an autocorrelation method at various points in the centre of the domain. The variation between the experimental and spectral turbulence is suitable, so the grid of generated velocities is used as the background ambient turbulence. The next stage is to outline the different conditions in which the turbine can operate and in particular those conditions which effected the experimental case.

D. Distortion of Turbulence

Using the turbulent flow field generate by the von Kármán energy spectra and extracting inflow velocity, results in no impact from the rotor onto the mean flow, the turbulence is considered locally 'frozen'. However, this is not the case if the rotor is actually present whilst rotating through the flow field, there is an additional non-zero mean strain component imposed upon the flow field. Previous work by [20] and [21], into examining the effect of the non-zero mean strain component shows that it can result in tilting, stretching and displacement of vorticity components. This has been examined for a bluff body by [22] through the use of rapid distortion theory. Initial work focussed on applying this theory to a contracting duct in a wind tunnel, [23], however the application for Tidal turbines is through the use of an actuator disc, a study has recently been conducted by [24].

The method applied here focusses on the distortion due to the small ratio of turbulent length scale to diameter, as with the study conducted by [24], the distortion is determined at a central point in the middle of the rotor in the flow field. The ratio of the mean square of the turbulent velocity is given in (2). This is determined using the RDT theory outlined in [23], with a Lagrangian specification of the motion of the flow.

$$\frac{\langle u^2 \rangle}{\langle u_\infty^2 \rangle} = \mu(c) = \frac{3}{4}\frac{(\sqrt{s} + (s-1)tan^{-1}(\sqrt{s}))}{c^2 s^{3/2}} \tag{2}$$

In Equation 2, $s = c^3 - 1$ where c is the contraction coefficient which for the actuator disc is less than one and is determined from $c = 1 - a$, with a being the axial induction. This gives an increased turbulence intensity of the flow field. A wave number method is also applied to give the variation across the velocity spectrum. The relationship between distorted and undistorted wave number is given by 3, which is obtained from [23].

$$\chi_i = \frac{\partial \xi_{j\infty}}{\partial x_i}\kappa_j \tag{3}$$

TABLE I
COMPARISON OF LENGTH SCALE BETWEEN EXPERIMENT AND SPECTRAL TURBULENCE

Symbol	Length scale (m)	Percentage Difference
Experimental	0.6	
von Kármán	0.5381	10

Where χ_i is the distorted wave number and κ_j is the undistorted. Considering only strain is at the centre of the rotor, the non-diagonal terms in the strain tensor are zero. This relationship follows through to a relationship between the spectral tensors (Φ_{11}) of the turbulence, shown in Equation 4.

$$\Phi_{11}(\kappa) = \frac{\kappa^4}{\kappa_\infty^4}\Phi_{11\infty}\kappa_\infty \tag{4}$$

Following through from this using the method in [24], the one-dimensional frequency spectrum is defined by Equations II-D and II-D, for the distorted and undistorted turbulence, respectively.

$$\phi_{11}(\kappa_1^*) = \frac{\kappa^{*4}\tau^{*3}d\tau}{2(c^{-2}\kappa_1^{*2} + c\tau^{*2})^2(1+\kappa_1^{*2}+\tau^{*2})^{17/6}} \tag{5}$$

$$\phi_{11\infty}(\kappa_1^*) = \frac{\kappa^{*4}\tau^{*3}d\tau}{\kappa^{*4}(1+\kappa_1^{*2}+\tau^{*2})^{17/6}} \tag{6}$$

Where $(c^{-2}\kappa_1^{*2} + c\tau^{*2})$ is the term to describe the distorted wave number, the turbulence energy function which has been used is the von Kármán, κ^* is the non-dimensional wave number, and $\tau^2 = \kappa_2^2 + \kappa_3^2$.

This results in a variation of the one-dimensional frequency spectra for the streamwise velocity with wave number. This variation is implemented to the velocity spectra extracted from the von Kármán grid of velocities. The results of the inclusion of this distortion are shown in Section III.

E. Shear Flow

One of the most common definitions of sheared flow at a tidal site is the power law profile, which uses a specific index to highlight the level of vertical shear. Vertical shear is caused by the surface roughness of the sea bed and therefore can vary with bathymetry. However in most tidal sites a 1/7th vertical shear profile has been found, [11], [18], [25] and [26]. In this investigation a range of power law shear profiles will be examined and compared to the experimental case.

In addition to vertical shear, disturbances in the flow field can cause a more transverse shear than only a variation due to turbulence. A brief study into a linear variation of shear across the transverse direction of the rotor plane is also included. Previous work in examining the flow field from the experimental case has shown that this slight linear variation may be present, [9].

F. Waves

The influence of waves onto the blade loading can be found by using the depth variation of velocity due to a series of wave spectra, with wave velocity at specific heights through the depth using (7).

$$U_{wave} = (\omega_r - kU_0)a_w\left(\frac{cosh(k(d+z))}{sinh(kd)}\right)cos(\phi - \omega_r t) \tag{7}$$

Where U_0 is the current velocity, a_w is the amplitude of the wave obtained using a Bretschneider spectrum,

d is the depth of water, z is the vertical position (-ve below the surface), ϕ is the phase and ω_r is the relative angular frequency defined by (8), with k corresponds to wave number which is relative the moving frame of reference.

$$\omega_r = U_0 k + \sqrt{gktanh(kd)} \tag{8}$$

Using the variation of velocity with depth the loading as been assessed with the a constant onset flow, to establish the variation in magnitude of the loads with frequency will depend solely on the waves, no turbulence.

G. Tower Shadow

Tower shadow is the term used to describe the influence of the tower onto the onset flow experienced on a rotor upstream. The influence of the tower causes a velocity deficit upstream and can be modelled using potential flow theory. The deviation of the flow around the tower causes a reduction in axial speed and a slight increase in lateral. The variation in flow speed is calculated depending on the blade location within the revolution, the equations which show the variation in lateral and axial onset flow for the lower half of the rotor are given by equations II-G and II-G

$$V_y = U_\infty \left(\frac{r_t^2}{d_{rs}^2} \right) sin(2\phi) \tag{9}$$

$$V_x = U_\infty \left(1 - \frac{r_t^2}{d_{rs}^2} \right) cos(2\phi) \tag{10}$$

Where V_x is the axial component and V_y is the lateral, d_{rs} is the distance of each blade segment to the tower centre, ϕ is angle between the blade segment and the tower and r_t is the tower radius. The dimensions used for determining the effect of tower shadow were taken from the experimental set up, leaving a ratio between tower diameter and rotor overhang of 0.099. This method for including the influence of tower shadow has been applied to wind turbines in [27], where the overhang ratios vary between 0.2 to 0.33 which have been found to effect the thrust by 4-8%. The influence of the tower shadow on the blade loading will be investigated.

III. Blade Loading

The loading considered in this study is the blade root bending caused by the axial load, M_x. Initially the procedure for determining the loading takes into account the initial grid of time varying turbulent velocity components, and imposes the various velocity deficits and spectral shifts due to the different operational conditions. With the new time-varying components the relative velocity and inflow angles are determine for ten positions along the blade, which rotates with angular frequency given by the chosen operating point. In this case for comparison with the experimental case a TSR of 5.89 is used.

To determine the axial loading a blade element approach is used, where (11-12) provide the time varying lift an drag force experienced at the ten positions along the blade and (13) provides the axial force at each position along each blade.

$$\delta L(t) = B\frac{1}{2}\rho c (U_{rel})^2 C_L \delta r \tag{11}$$

$$\delta D(t) = B\frac{1}{2}\rho c (U_{rel})^2 C_D \delta r \tag{12}$$

$$\delta F_a(t) = \delta L(t) cos(\phi(t)) + \delta D(t) sin(\phi(t)) \tag{13}$$

In all cases here a constant axial induction has been used which corresponds to the induction included for the turbulence distortion. The lift and drag data has initially been taken from a CFD simulation for a blade segment corresponding to the experimental case, in steady conditions, at the appropriate Reynolds number.

H. Blade Scale Flow

This section focusses on the load magnitude at the high frequency end of the load spectra. As shown in Fig. 2, it is considered here that fluctuations at the blade scale result in the increased magnitude, whereas currently the load spectra defined follows a -5/3 decay of the energy within the turbulent flow field. This difference in magnitude is most noticeable when the overall load cycles are determined.

In this study the fluctuations at blade scale have been approximated by terms describing the fluctuations of lift and drag coefficient that arise when a 2D blade segment is subject to an unsteady inflow. This variation due to relative velocity from onset turbulence has been assessed to inform the evaluation of the onset turbulence method on the frequency variation of blade and turbine loads. A NACA 63-818 profile (as the profile at 0.7R from [9]) is studied using a RANS k-ω SST solver. A C-shape mesh was created around the aerofoil, this allows for varying angular inflow without any disturbances at the upper and lower boundaries. Grid convergence was examined using Richardson extrapolation, initially at a Reynolds (Re) number of 800k for comparison with experimental data from [28]. From this comparison the lift and drag results obtained were in better agreement with the experimental data than XFoil. The convergence was then re-checked with a lower Re number of 181k, in line with the Reynolds number local to the blade at 70% radius chosen from the experimental case in ([9]). In comparison with XFoil results at the same Re number the ratio between the two forces are in better agreement with the higher Re with Xfoil producing a much higher ratio in both cases. In each of the simulations conducted for the mesh convergence study there is a higher level of refinement surrounding the aerofoil and a scale ratio between cells no greater than 1.2.

Initially a steady inflow velocity is used to define the variation of lift and drag over a range of angles of attack, as shown in Fig. 3. This is used in the initial determination of blade loading. Then the relative velocity experienced by a blade at 0.7R is used as the onset flow, the varying lift and drag coefficients are obtained for 25 rotations of the blade at numerous

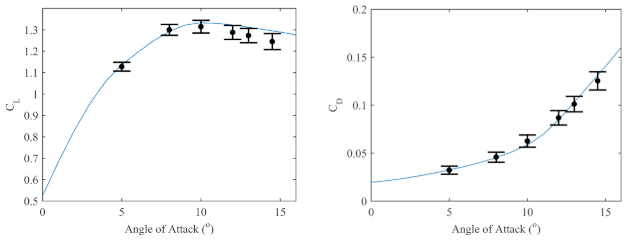

(a) Lift Coefficient (b) Drag Coefficient

Fig. 3. Variation of force coefficients with angle of attack, steady conditions (blue line), range of coefficients from unsteady conditions (black bars), mean coefficients from unsteady conditions (black dot).

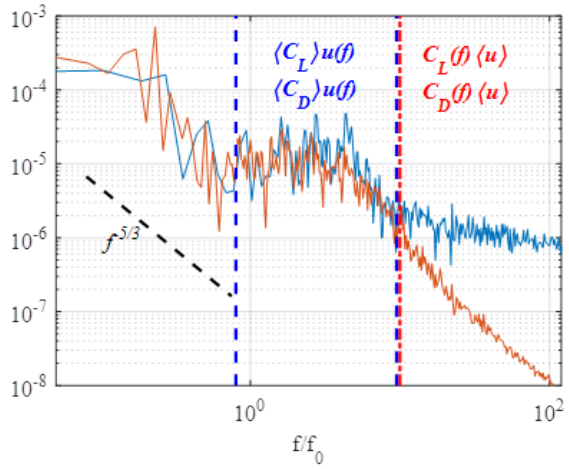

Fig. 4. Example of spectra of lift coefficient at 14^o (blue) with fluctuating component of the onset relative velocity (orange), this spectra is divided into, low, mid and high frequency ranges, with the key areas of influence for the magnitude of the unsteady lift and drag, in the mid range only a mean lift and drag are considered, in the high frequency range the magnitude of the fluctuating part is used in conjunction with the mean velocity and aggregated onto the original load spectra.

angles of attack, a selection of angles and the range of coefficient is also shown in Fig. 3.

The spectra of the CFD predictions of time-varying lift and drag are then compared to the spectra of onset relative velocity fluctuations. An example is shown in Fig. 4, this compares the lift coefficient at an angle of attack of 14^o to the fluctuating velocity, the spectra has been divided into three separate frequency bands, this is to highlight the dominant fluctuating components. For the low and high frequency range the fluctuating component of velocity follows the energy decay trend of -5/3, this is expected. In the mid-frequency range highlighted by the blue lines, the magnitude of the lift and velocity are very similar, only in the high frequency range is there any variation between the two magnitudes, highlighted by the red lines. This variation shows that there is an increase in the magnitude due to the lift coefficient, hence the force coefficients are considered to dominate in this range and can be combined with the mean velocity to determine additional loading. The frequency at which the lift force spectra diverges from the velocity spectra is dependant on the inflow angle to the blade, in this study the separation between the lift and velocity is considered to occur at approximately $10f_0$ for all positions along the blade in this case.

IV. Evaluation of Unsteady Flows

This section evaluates the influence of different operational conditions onto a load spectra generated from a quasi-steady flow case. These spectra have been compared to experimental results generated as part of the XMED tests (Extreme Loading of Marine Energy Devices due to Waves, Current, Flotsam and Mammal Impact). The experimental set up and turbine specification are detailed within [29]. The tests performed here focussed upon the variation of loading at two turbulence intensities The experimental data used here focuses the root bending moment data obtained for the low turbulence case at 3% intensity, and wave loading from a specific set of regular wave conditions.

I. Loading due to onset turbulence

Firstly the effect of turbulence distortion onto the blade loading spectra is investigated. Fig. 5 shows shift in magnitude of the load spectra with the addition of distortion, over the mid to high frequency range this reduces and follows the magnitude of the experimental spectra.

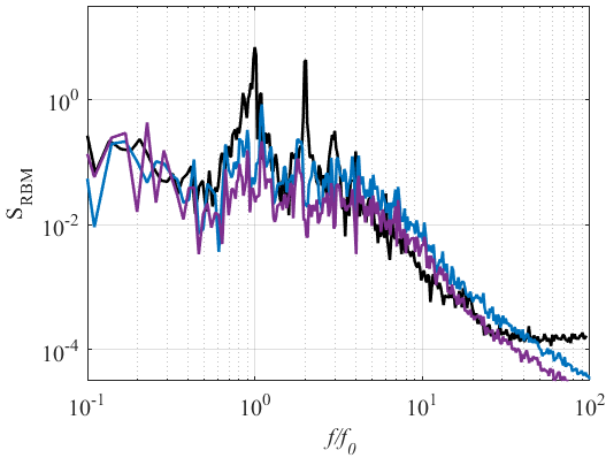

Fig. 5. Blade loading, one blade only in each case, experimental (black), induction only (blue), induction with distortion (purple).

Including the distortion has resulted in an overall decrease in the magnitude of the spectra shown in Figure 5. It has also had no impact on the magnitude at the peaks of the rotor harmonics as there is no periodicity. Tower shadow is then implemented and the load spectra is shown in Fig. 6. By including the tower shadow the peak at the rotor frequency has increased by a factor of 62.25, however this is still not the magnitude of the experimental case, hence various shear profiles will be applied next in addition to tower shadow and distortion.

The next factor investigated was vertical shear, as mentioned previously the onset flow field has been examined in recent work and an obvious 1/7th shear profile was not found to be present. The variation in peak loading for a range of shear profiles has been

TABLE II
COMPARISON OF THE MAGNITUDE OF PEAK LOADING, BETWEEN DIFFERENT TRANSVERSE CASES AND THE EXPERIMENT.

Transverse Variation (%)	Percentage Difference
1.5	41.7
2	0.83
2.25	23.7
2.5	51.2

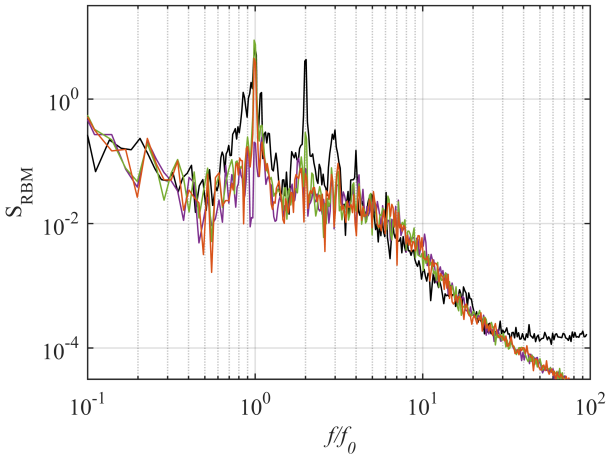

Fig. 6. Blade loading, one blade only in each case, experimental (black), induction with distortion and tower shadow (purple), added vertical shear (1/20th) (green), with no vertical shear, but added linear transverse variation of 2% (orange).

examined in [10], corresponding with this work a smaller profile of 1/20th has been included here. This shear profile is applied as a constant over the velocity grid with time and hence has a strong periodic nature, this is shown in Fig. 6.

The peak produced from the vertical shear profile with induction and distortion is within 85% of the experimental case. The linear deficit referred to as transverse shear has been applied for a range of percentages, around 2%, which has been observed in the experimental set up [9]. By applying these percentages the peak loading at the rotor frequency varies as shown in Table IV-A.

Applying just a transverse variation of 2% across the rotor plane produces a blade averaged peak load within 1% of the experimental case. When examining the load spectra, even with the operational conditions included, there is a lack of magnitude in the peaks at the rotor harmonics.

There a various reasons why the peaks do not agree, one is the spatial resolution of the velocity grid and potentially the number of points extracted per blade could effect the overall magnitude and variance of the spectra, causing a slight reduction across the peaks. Another could be neglecting induction caused by a steel beam used at the bed of the turbine, which the turbine was mounted behind in the experiment.

Due to the agreement between the linear variation from a 2% profile and the experimental data, vertical shear of 1/20th is not included any further analysis of a single turbine.

J. Loading due to Blade-Scale flow

Based upon the understanding of the lift and drag spectra shown in the previous section, the magnitude of the fluctuations for the lift and drag coefficients ($> 10f_0$), is then reintroduced to the blade element method used previously to recalculate the contribution to the root bending moment on each blade. The addition of considering the contribution due to the blade scale flow is shown in Fig. 7. In the high frequency range ($> 10f_0$) there is a noticeable shift in the spectral magnitude, the difference in load cycles and DEL for this shift are shown in the following section.

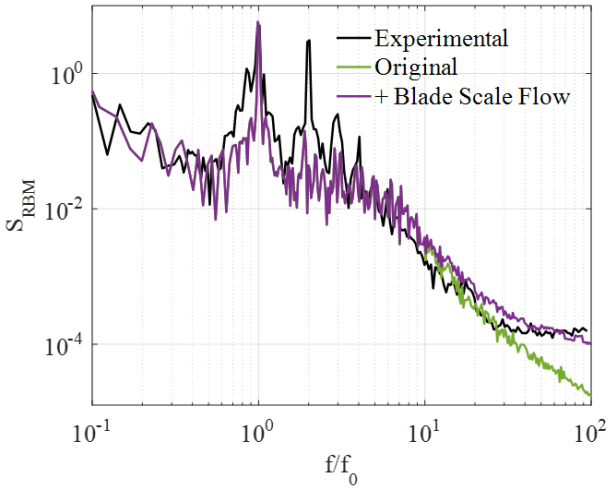

Fig. 7. Blade loading, one blade only in each case, experimental (black), induction with distortion, tower shadow and transverse shear (2%) (green), with blade scale fluctuations from the magnitude of the unsteady lift and drag components (purple)

K. Loading due to Waves

The loading due to waves is examined using the depth variation of velocity with time. To determine the accuracy of the method a comparison will be made to experimental results from the same series of tests, using the 1.2 m diameter turbine. One wave case has been chosen, with a wave amplitude of 0.11 m, a frequency of 0.89 Hz and a constant rotational speed of 70 rpm. The resultant load spectra for the wave is based upon the thrust force experienced by the rotor. This is property chosen for comparison as there are no blade loading results for waves from the experimental case. The spectra of thrust is shown in Fig. 8, considering waves occurring with constant onset flow and no turbulence, compared to waves with a 3% turbulence domain (in this case from the von Kármán method) and to the experimental results.

Considering the constant onset flow case the peak magnitudes at the wave frequency and first harmonic are within +/- 6% of the experimental peak values for the thrust force. By introducing the 3% turbulence to the inflow the overall variance of the data increases, this leads to larger fluctuations and the increase to the spectra, which corresponds to the magnitude in the

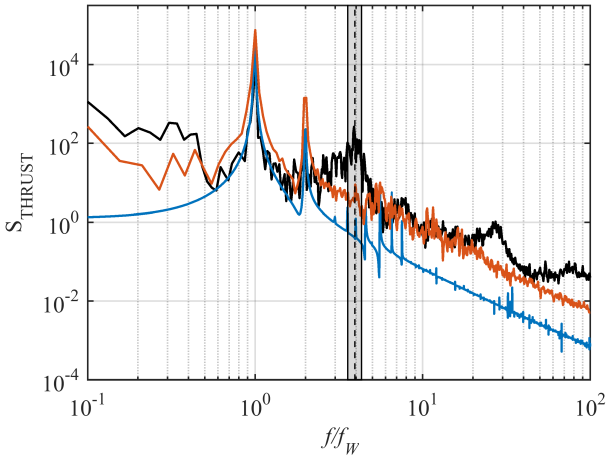

Fig. 8. Rotor loading, experimental (black), influence of waves with constant onset velocity (blue), with 3% turbulence and added linear transverse variation of 2% (orange), band to show variance for experimental case around $3f_0$.

mid-frequency range of the experimental spectra. The total energy in the mid to high frequency ($10f/f_W - 100f/f_W$) range is not replicated by the inclusion of the turbulence, with a 10% increase in energy between the non-turbulent to turbulent case, however this is still lower than the experimental case by a factor of 2.8. Also the peak magnitudes for the turbulent case are larger for the wave frequency and first harmonic by a factor of 3.6 and 9.7, respectively. The loading due to waves is an area for more consideration, as the turbulence is constructively interfering with the spectra of velocity from waves hence causing larger loads than the turbine should experience. Further examination into the experimental conditions shows the potential for an increase in turbulence intensity The effect of the turbulence with the waves on the load cycles will also be examined in the next section.

L. Load Cycle Analysis

Load spectra analysis has been conducted to gather an understanding of the impact of different operational conditions across various frequency ranges. Corresponding to each spectra of load is a time history which can be used as an input to a Rainflow calculation of load cycles. This method is used when the load is not a simple periodic time series, but rather a more complex irregular variation of stress reversals, the method is described well in [30]. The resultant variation in load cycles is shown in Fig. 9(a) and (b) for the blade loading, there is a 17% different between the total number of load cycles. This highlights the reduction in higher magnitude cycles for the spectral case, as the number of cycles at the lowest cyclic range is within 5%.

Using the data gathered from the Rainflow counting the damage equivalent loads can be determined, using (1). The damage equivalent load has been determined for the different blade loading cases with the inclusion of tower shadow providing an oscillating load magnitude within 44% of the average experimental. With the

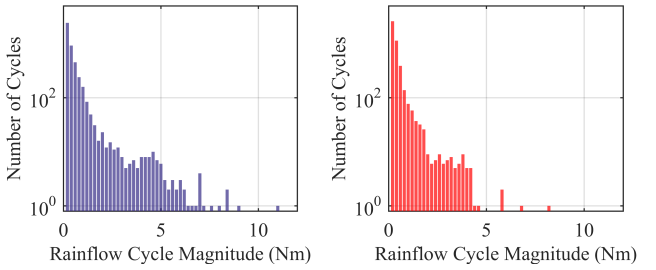

(a) Experimental (b) Operational Conditions including 2% linear variation

Fig. 9. Variation of load cycles between, (a)experimental root bending moment data and (b) root bending moment from turbulence spectra with applied operational conditions.

addition of the linear variation at 2% the DEL is within 22%. As this value is directly effected by the magnitude of the number of load cycles, a better prediction of load cycles is needed. Rainflow cycle counting method is then performed on the time history of loads based upon the load spectra with blade scale flow included. This results in the number of total cycles to increasing to within 1% of the experimental case. This should result in an increase in DEL, which it does by 2%, bringing the DELs to within 20% of the experimental value. This increase is not as significant as the load cycles, due to the lack of magnitude around the rotor harmonics for the spectral turbulence case.

For the rotor loading due to waves the variation of load cycles is given in Figure 10. The distribution of loads varies between the different load spectra, for the experimental case there is a larger number of small cycle magnitude than the constant onset and turbulent wave cases, there is a bimodal trend for each case with the second mode - increase in cycles occurring at a lower cycle magnitude than the turbulent wave case, these correspond to the increase in peak loading. For rotor loading due to waves, with no turbulence the DEL is found to be 40% lower than the experiment, and with the inclusion of turbulence the DEL is 29% greater. This over prediction will be influenced by the increase higher magnitude cycles, the under prediction will be influenced primarily by the lack of cycles across

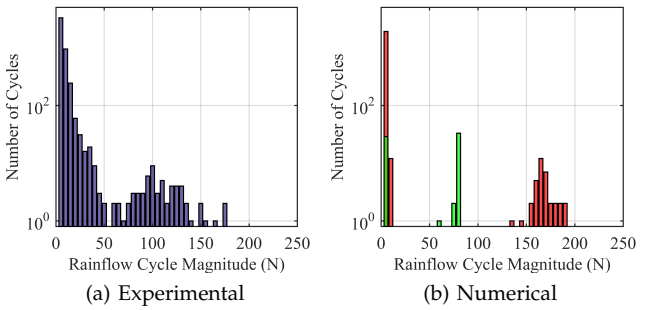

(a) Experimental (b) Numerical

Fig. 10. Variation of load cycles between, (a) experimental root thrust data and (b) wave loads with constant onset U_0 (red) and wave loads with applied turbulence at 3% and linear transverse shear at 2% (green).

the magnitudes.

For rotor loading due to waves, with no turbulence the DEL is found to be 40% lower than the experiment, and with the inclusion of turbulence the DEL is 29% greater. This over prediction will be influenced by the increase higher magnitude cycles, the under prediction will be influenced primarily by the lack of cycles across the magnitudes.

V. Discussion

Longer term loading is important for overall fatigue life calculations. As mentioned in the introduction the understanding of loading at one quasi-steady condition can be used to determine the loading over a range of sea-states. In this case a brief example of the loading experienced over a 30 day period is given, where each load spectra is determined with varying onset mean velocity flow fields and turbulence intensity. The range of velocity and turbulence intensity is given in Fig. 11. This has been determined using 9 tidal constituents from the Pentland Firth, which is shown in Fig. 1.

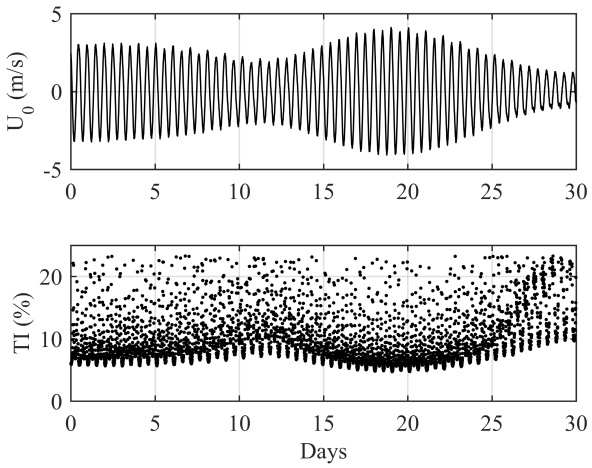

Fig. 11. Top: Time varying mean onset flow modelled from a tidal site, Bottom: Time varying turbulence intensity modelled from trend with literature and mean velocity, for method see [15].

In this case the von Kármán spectral turbulence has been generated using a Froude scaled version of this variation of mean onset flow and turbulence intensity. Some operational factors have been included such as tower shadow and stretching, however vertical and transverse shear have not been applied. The aim here is to determine the variation of loads due to the levels of turbulence over this 30 day period and compare the results here with previous results where a scaled experimental spectra has been used, [15]. The DELs and load cycles are calculated for the blade loading at each quasi-steady state and then aggregated for the 30 day period. This variation of DEL for the semi-flexible material are shown in Fig. 12. This variation is shown for the quasi-steady intervals where the mean onset flow is above 0.5 m/s and the TSR is constant for maximum rated power, for this 30 day period that results in 76% of the original data set being used.

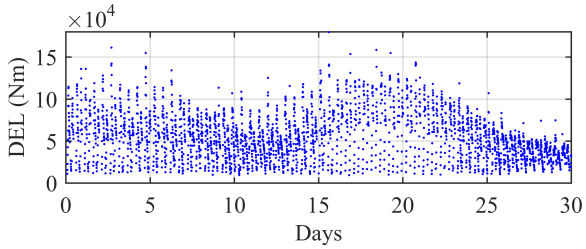

Fig. 12. Preliminary results for damage equivalent loads determined for a semi-flexible material for blade loading, determined at each quasi-steady interval over a 30 day period.

VI. Conclusions

- Single peak blade loading at the rotor frequency can be reproduced to within 1% of the experimental data.
- Peak magnitudes of thrust due to wave loading can be predicted within 6% of experiment, using a constant plug flow.
- From the blade loading study, the magnitude of subsequent peaks at rotor harmonics are not captured here with the inclusion of periodic components such as tower shadow, transverse and vertical shear.
- The damage equivalent loads vary by 22%, without the inclusion of blade scale fluctuations in force coefficient this improves to within 20% with the inclusions of blade scale fluctuations. Again, the loss of magnitude at the rotor harmonics of the blade loading may account for the overall difference.
- Turbulence is found to act constructively with wave spectra which results in an over-estimation of the peak loading on a rotor due to thrust.

This method is quick at producing a close prediction of blade loads, when compared to experimental results. It can be applied to a range of site specific design conditions, which allows for the optimisation of the turbines within the site based upon the fatigue loading of different components. Understanding the variation in loads due to unsteady environmental conditions can influence locations of turbines within arrays and within site locations. If there is a potential for 100 turbines within site, using this process, different areas of the site can be considered. With the opportunity to design the locations of turbines based upon which parts of the site will give an equal length of design life.

Further work needs to be conducted into the influence of operational loads on the rotor loading and investigating the onset flow in more detail to determine the peak magnitudes at the rotor harmonics. In addition long term full scale wave conditions will be investigated using the synthetic turbulence case and compared to results from using scaled experimental spectra.

Acknowledgement

Thanks to DNV-GL who provided a research license to allow the use of Tidal Bladed and to George Crossley for providing the extraction code for the Tidal

Bladed data. The experimental results were conducted as part of the XMED project supported by EPSRC (EP/J010235/1).

REFERENCES

[1] O. Faltinsen, "Wave Loads on Offshore Structures," *Annual Review of Fluid Mechanics*, vol. 22, pp. 35–56, 1990.

[2] P. Veers, *Fatigue loading of wind turbines*. Woodhead Publishing Limited, 2009. [Online]. Available: http://dx.doi.org/10.1533/9780857090638.1.130

[3] B. Sellar and D. Sutherland, "Tidal energy site characterisation at the Fall of Warness, EMEC, UK," Tech. Rep., 2015.

[4] B. Gaurier, P. Davies, A. Deuff, and G. Germain, "Flume tank characterization of marine current turbine blade behaviour under current and wave loading," *Renewable Energy*, vol. 59, pp. 1–12, 2013. [Online]. Available: http://dx.doi.org/10.1016/j.renene.2013.02.026

[5] P. Mycek, B. Gaurier, G. Germain, G. Pinon, and E. Rivoalen, "Experimental study of the turbulence intensity effects on marine current turbines behaviour. Part I: One single turbine," *Renewable Energy*, vol. 66, pp. 729–746, 2014. [Online]. Available: http://dx.doi.org/10.1016/j.renene.2013.12.036

[6] I. Afgan, J. McNaughton, S. Rolfo, D. Apsley, T. Stallard, and P. Stansby, "Turbulent flow and loading on a tidal stream turbine by LES and RANS," *International Journal of Heat and Fluid Flow*, vol. 43, pp. 96–108, 2013. [Online]. Available: http://linkinghub.elsevier.com/retrieve/pii/S0142727X13000672

[7] U. Ahmed, D. Apsley, I. Afghan, T. Stallard, and S. P.K., "Fluctuating Loads on a Tidal Turbine Due to Velocity Shear and Turbulence: Comparison of CFD with Field Data." *Renewable Energy*, 2016.

[8] DNV-GL, "Standard Tidal Turbines (DNVGL-ST-0164)," no. October, 2015.

[9] G. S. Payne, T. Stallard, R. Martinez, and T. Bruce, "Variation of loads on a three-bladed horizontal axis tidal turbine with frequency and blade position," *Journal of Fluids and Structures*, vol. 83, pp. 156–170, 2018. [Online]. Available: https://doi.org/10.1016/j.jfluidstructs.2018.08.010

[10] H. Mullings and T. Stallard, "Unsteady loading in a tidal array due to simulated turbulent onset flow," in *3rd International Conference on Renewable Energies Offshore*, 2018.

[11] G. N. McCann, R. I. Rawlinson-smith, and K. Argyriadis, "Load Simulation for Tidal Turbines using Wind Turbine Experience," *GH Tidal Bladed*, no. 1870, p. 10, 2007.

[12] F. Elasha, D. Mba, J. A. Teixeira, and M. Togneri, "Life Prediction of Tidal turbine Gearboxes," in *Proceedings of 11th European Wave and Tidal Energy Conference, Nantes, France*, 2015, pp. 2–9.

[13] T. Blackmore, L. E. Myers, and A. S. Bahaj, "Effects of turbulence on tidal turbines: Implications to performance, blade loads, and condition monitoring," *International Journal of Marine Energy*, vol. 14, pp. 1–26, 2016. [Online]. Available: http://www.sciencedirect.com/science/article/pii/S2214166916300297

[14] P. W. Galloway, L. E. Myers, and A. S. Bahaj, "Quantifying wave and yaw effects on a scale tidal stream turbine," *Renewable Energy*, vol. 63, pp. 297–307, 2014. [Online]. Available: http://www.sciencedirect.com/science/article/pii/S0960148113004977

[15] H. R. Mullings, T. J. Stallard, and G. S. Payne, "Operational Loads on a Tidal Turbine due to Environmental Conditions," in *27th International Offshore and Polar Engineering Conference*, no. 939, 2017, pp. 1–14.

[16] G. Freebury and W. Musial, "Determining equivalent damage loading for full-scale wind turbine blade fatigue tests," *2000 ASME Wind Energy Symposium*, no. February, p. 12, 2000. [Online]. Available: http://arc.aiaa.org/doi/abs/10.2514/6.2000-50

[17] J. G. Leishman, "Challenges in modelling the unsteady aerodynamics of wind turbines," *Wind Energy*, vol. 5, no. 2-3, pp. 85–132, 2002. [Online]. Available: http://doi.wiley.com/10.1002/we.62

[18] T. Burton, N. Jenkins, D. Sharpe, and E. Bossanyi, *Wind Energy Handbook*, 2011. [Online]. Available: http://books.google.com/books?hl=en\&lr=\&id=dip2LwCRCscC\&pgis=1

[19] J. Melorose, R. Perroy, and S. Careas, "Tidal Bladed Theory Manual," Tech. Rep., 2015.

[20] L. Prandtl, "Attaining a Steady Air Stream In Wind Tunnels," Tech. Rep. No. 726, 1933.

[21] G. I. Taylor, "Turbulence in a contracting stream," *Z.a.M.M*, vol. 15, no. 1-2, pp. 91–96, 1935.

[22] J. C. R. Hunt, *A theory of turbulent flow round two-dimensional bluff bodies*, 1973, vol. 61, no. part 4.

[23] G. K. Batchelor and I. Proudman, "The effect of rapid distortion of a fluid in turbulent motion," *Quarterly Journal of Mechanics and Applied Mathematics*, vol. 7, no. 1, pp. 83–103, 1954.

[24] J. M. Graham, "Rapid distortion of turbulence into an open turbine rotor," *Journal of Fluid Mechanics*, vol. 825, pp. 764–794, 2017.

[25] P. O. Okorie, A. Owen, P. Pollard, and M. Hossain, "Study of Coherent Structures Suitable for Numerical Testing of Tidal Current Energy Devices." *EWTEC 2011 Proceedings*, 2011.

[26] M. Togneri, I. Masters, and J. Orme, "Incorporating Turbulent Inflow Conditions in a Blade Element Momentum Model of Tidal Stream Turbines," in *Proceedings of the Twenty-first (2011) International Offshore and Polar Engineering Conference*, vol. 8, 2011, pp. 757–762.

[27] E. Smilden, A. Sø rensen, and L. Eliassen, "Wind Model for Simulation of Thrust Variations on a Wind Turbine," *Energy Procedia*, vol. 94, no. 1876, pp. 306–318, 2016. [Online]. Available: http://dx.doi.org/10.1016/j.egypro.2016.09.188

[28] Q. Guo, L. Zhou, and Z. Wang, "Comparison of BEM-CFD and full rotor geometry simulations for the performance and flow field of a marine current turbine," *Renewable Energy*, vol. 75, pp. 640–648, 2015. [Online]. Available: http://dx.doi.org/10.1016/j.renene.2014.10.047

[29] G. S. Payne, T. Stallard, and R. Martinez, "Design and manufacture of a bed supported tidal turbine model for blade and shaft load measurement in turbulent flow and waves," *Renewable Energy*, vol. 107, pp. 312–326, 2017. [Online]. Available: http://linkinghub.elsevier.com/retrieve/pii/S0960148117300782

[30] S. D. Downing and D. F. Socie, "Simple rainflow counting algorithms," *International Journal of Fatigue*, vol. 4, no. 1, pp. 31–40, 1982.